Molecular Motion in a Crystalline Analogue of Bisphenol-A Polycarbonate

P. Mark Henrichs*

Corporate Research Laboratories, Eastman Kodak Company, Rochester, New York 14650

Henry R. Luss

Analytical Technology Division, Eastman Kodak Company, Rochester, New York 14650

Raymond P. Scaringe

Life Sciences Research Laboratories, Eastman Company, Rochester, New York 14650. *Received August 29, 1988; Revised Manuscript Received December 9, 1988*

ABSTRACT: The diphenol carbonate of 2,2-bis(4-hydroxyphenyl)propane is a small-molecule analogue of bisphenol-A polycarbonate. X-ray structures of two crystal forms have been determined. Deuterium NMR spectroscopy shows that both the inner and the outer rings in one of these forms undergo facile 180° flips. There are two populations of inner rings in the mobile form, however, one flipping at a much faster rate than the other. X-ray crystallography confirms that there are two types of molecules in the crystal. Detailed analysis of the deuterium spectra of the mobile crystalline form at temperatures between 305 and 350 K indicates that ring flipping is accompanied by a secondary, low-amplitude motion that can be approximated as ring wiggling about an axis perpendicular to the ring. A model is proposed for ring flipping in the model compound and in the polymer in which ring motion is tightly coupled into the motion of the carbonyl group. Analysis of the crystal structure of the mobile form verifies that the carbonyl carbons in one type of molecule interact strongly with neighboring molecules while those in the other type of molecule do not. The connection between the motion of different parts of the model-compound molecule explains why mechanical spectroscopy, dielectric relaxation, and NMR spectroscopy give parallel results for bisphenol-A polycarbonate.

Introduction

An important property of bisphenol-A polycarbonate (BPAPC) is that it has high impact strength well below

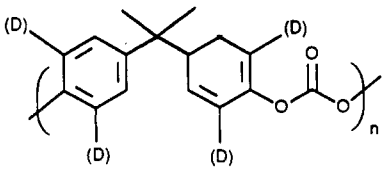

BPAPC (optionally deuteriated)

its glass transition temperature of 150 °C. It has been proposed that prominent localized motions in BPAPC serve to dissipate energy below T_g and thus account for the impact strength of the polymer.[1-3] A considerable body of circumstantial evidence supports this concept.[4-12] The low-temperature ductility of polycarbonate also appears to be related to the local molecular motions.[13-18]

The mechanical properties of blends of BPAPC with other polymers sometimes differ from the properties predicted by a simple linear sum of the properties of the individual components.[19] If localized motions in BPAPC help determine its bulk physical properties, modification of these in the blend could lead to properties of the mixture not characteristic of either of the pure components. Understanding how one polymer can influence the dynamic properties of another with which it is blended will aid in the design of polymer blends with advantageous physical properties.

Although the presence of prominent mechanical loss peaks at low temperature is a direct consequence of local motions in the individual chain fragments of polycarbonate,[20-22] considerable controversy has existed as to the exact nature of the motions. Inferences about what chemical moieties are responsible for the mechanical loss peaks must be made through comparison of results for a large series of structurally different polymers. Yee and Smith summarized much of the existing literature on mechanical spectroscopy of derivatives of BPAPC in 1981 and proposed that the primary mechanically active motion in polycarbonate is a cooperative reorientation of both the phenyl rings and the carbonate group.[21] The large dielectric loss peak observed at low temperatures confirms that considerable motion of the dipolar carbonate group occurs.[22,23]

Changes in the broad-line proton NMR[24-28] spectrum with temperature also show that there is considerable mobility of the phenyl rings in BPAPC. Only in selected derivatives of BPAPC is the proton spectrum simple enough that conclusions about the details of motion may be made, however.[29]

Measurements of ^{13}C nuclear relaxation times in solid BPAPC complement the proton results but still do not fully clarify the nature of the motions.[30-32] The most detailed information about motion in BPAPC has come from deuterium[33-36] and carbon[27-42] NMR line-shape studies.

The primary motion in BPAPC to which NMR is sensitive is a 180° flip of the aromatic rings. A distribution of ring-flipping rates spanning 3 orders of magnitude at room temperature[33,34,37-40,42] has been detected. By itself, ring flipping is uninteresting in that it leads to no net energy absorption by the system. Nevertheless, the presence or absence of ring flipping in polycarbonates and other polymers with aromatic rings in the backbone correlates well with the presence or absence of low-temperature mechanical relaxations.[33,43] The ring flips appear to be coupled to mechanically active motions. Both motions within the polymer lattice[43,44] or interchange of cis–trans and trans–trans conformations of adjacent carbonate groups in the polymer chain[45] have been proposed as the mechanically active process. Deuterium and carbon NMR spectra of polycarbonates are affected by a secondary process in addition to ring flipping that has been described as a high-frequency, low-amplitude oscillation of the rings about the 1,4 axis.[33-35,37-40]

Recently one of us coauthored a paper on a crystal structure for the diphenyl carbonate of 2,2-bis(4-hydroxyphenyl)propane (I), a small-molecule analogue of BPAPC.[46] We have now examined I as a possible motional model for BPAPC. Unfortunately, ring flipping is very slow in the crystal structure first reported. Nevertheless, ring flipping is facile in a second crystal modification,[47] whose structure is presented herein. The fact that the rate

0024-9297/89/2222-2731$01.50/0

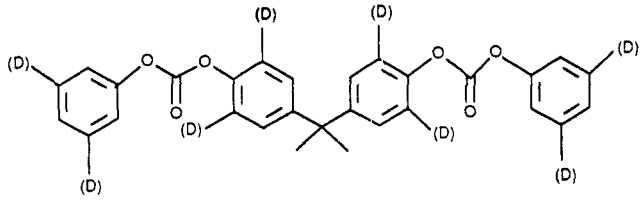

I

of ring flipping in I is drastically different for different packing environments gives us the opportunity to clarify the way in which chain packing affects motion in BPAPC. The two crystal forms of I will be referred to subsequently as immobile and mobile.

The mobility of the rings in I also has some general interest. Ring flipping occurs in a number of macromolecular materials other than BPAPC, including polystyrene,[48] polyesters based on terephthalic acid,[49] and the tyrosine[50-52] and phenylalanine[53] moieties of peptides and proteins. Ring flipping has also been observed in crystalline phenylalanine[53,54] and in crystalline peptides containing tyrosine,[50,52] but there is no previous report of ring flipping in crystalline compounds in which the rings are tied down at both ends.

Experimental Section

Bisphenol-A-d_4 was prepared by exchange of the 2, 2′, 6, and 6′ protons of perprotiobisphenol-A with an excess of deuterium chloride (35% in D_2O, Merck) in anhydrous ethyl ether at room temperature for approximately 2 weeks. The acid phase was replaced with fresh deuterium chloride solution, and the process was repeated. Workup and several recrystallizations from toluene led to needlelike crystals melting at 155–156 °C. Proton NMR spectroscopy and mass spectral analysis indicated that the product consisted of approximately 85% bisphenol-A-d_4 and 15% bisphenol-A-d_3.

Phenol-3,5-d_2. A mixture of phenol-d_6 (98.7 at. % deuterium, Merck), concentrated HCl (13% excess), and ethyl ether was refluxed for 100 h. The clear solution was then saturated with NaCl and extracted with several portions of dichloromethane. The combined extracts were washed with water and dried over $MgSO_4$. The product (mp 40–41 °C) was isolated by evaporation of the solvent and recrystallized from pentane. The proton NMR spectrum indicated it contained in excess of 93% at. % H at positions 2, 4, and 6.

The synthesis of I from bisphenol-A and phenyl chloroformate is described in the literature.[55] The preparation of the compound with deuterium in the outer rings exemplifies the method used for both types of deuteriated material. A solution of phenol-3,5-d_2 and a slight excess of pyridine in benzene was stirred rapidly in an ice bath. To this was added dropwise a solution of 0.95 equiv of bisphenol-A dichlorocarbonate in benzene. The creamy reaction mixture was allowed to warm slowly to room temperature and then was stirred overnight. Ethyl ether was added to effect separation of the liquid layers. The organic layer was washed first with 10% HCl and then with water, until the washes were neutral. Following drying over $MgSO_4$ and stripping of the solvent, the crude product was chromatographed through silica gel. The purest fractions were recrystallized from ethanol (mp 105–106 °C).

Bisphenol-A-d_4 Polycarbonate. The deuteriated monomer was polymerized with phosgene in dichloromethane and pyridine in the conventional manner. The resulting solution was washed well with HCl and water, and the polymer was precipitated in a large volume of 2-propanol. The sample was redissolved in dichloromethane, reprecipitated, and thoroughly dried under vacuum (T_g = 159 °C by differential scanning calorimetry (DSC), inherent viscosity 1.55 at 0.50 g/dL in CH_2Cl_2 at 25 °C, M_w 377 000, M_w/M_n 4.61 by gel permeation chromatography (GPC) as a styrene equivalent.)

Crystal Preparation. The immobile crystal form of I was obtained from slow crystallization from isopropyl alcohol with just enough acetone added to dissolve the compound, or from isopropyl alcohol with added dichloromethane. The melting range of this form was 102–105 °C.

Table I
Summary of Crystal Data and Refinement Parameters for the Mobile Form

formula	$C_{29}O_6H_{24}$
MW	468.51
space group	$C2$
cell constants at 23 (1) °C	
a, Å	29.84 (8)
b, Å	6.581 (3)
c, Å	12.888 (2)
β, deg	97.50 (9)
V, Å^3	2509 (9)
no. molecules/unit cell (Z)	4
D(calcd), g cm^{-3}	1.240
crystal dimensions, mm	0.08 × 0.36 × 0.48
absorption coeff (μ, Mo Kα), cm^{-1}	0.81
scan technique	ω
scan rate, deg min^{-1}	2.7–20
2θ limit, deg	50
hkl range	0 to 26, 0 to 5, −11 to +11
no. of unique data measured	2426
no. of data used in refinement ($I > \sigma(I)$)	1289
no. of parameters	316
$R = \sum\|\|F_o\| - K\|F_c\|\|/\sum\|F_o\|$	0.066
$R_w = (\sum w(\|F_o\| - K\|F_c\|)^2/\sum wF_o^2)^{1/2}$	0.064
$S = [(\sum w(\|F_o\| - K\|F_c\|)^2/(n_o - n_v)]^{1/2}$	1.33
wt parameters ($w^{-1} = \sigma^2(F_o) + (pF_o)^2 + q$)	
p	0.02
q	1.0
scale factor K	1.163 (3)
maximum shift in final cycle (Δ/σ)	0.07
residual e$^-$ density in final difference Fourier synthesis, e$^-$/Å^3	−0.17 to +0.18

The mobile crystalline form of I precipitated from a saturated solution of I in isopropyl alcohol with added dichloromethane as it cooled from the boiling point. The melting range was 104–106 °C. Numerous attempts to grow large crystals of the mobile form by slow evaporation under various conditions always led to the immobile form. The rapidly formed crystals were, of course, small, but one suitable for X-ray analysis was found.

Mass spectral analysis showed that both types of crystals were free from solvent. Differential scanning calorimetry verified that the melting range for the immobile form was greater than that for the mobile form but gave no indication that either form was contaminated with an amorphous component; the integrated areas of the melting endotherms for the two forms were equal. The correspondence of the crystals in the deuteriated powders actually used for NMR spectroscopy and the crystal of the immobile form used for X-ray analysis was verified by comparison of the predicted X-ray powder diffraction patterns and an experimental pattern.

The crystal structure of the mobile form was determined from X-ray data collected on an Enraf-Nonius CAD4 diffractometer. Details of crystal data and refinement are summarized in Table I. Programs used for data collection and structure solution and refinement are from the Structure Solution Package, SDP, V3.0, of the Enraf-Nonius Corp. (Delft, Holland).

Though there was initially an ambiguity among space groups $C2$, Cm, or $C2/m$, and the E statistics ($\langle E \rangle$ = 0.739, $\langle E^2 - 1 \rangle$ = 0.999) had a centric distribution, the structure was eventually solved and refined successfully in space group $C2$. There are two half-molecules in the asymmetric unit, each occupying a 2-fold symmetry site. Subsequently, we refer to the two types of molecules in the crystal as A and B. The MULTAN phase set having the second-best combined figure of merit gave a map containing 25 of the 36 non-hydrogen atoms. The remaining were obtained from a subsequent difference electron-density map. Because there was a low number of observed reflections, we decided to include hydrogen atoms constrained to ride on the parent carbon atoms at calculated positions.

Calculations of Intermolecular Interactions. The like neighbors of a given molecule (for example, an A molecule) were found by generation of all symmetry-equivalent molecules in the reference cell and all translates of these in surrounding cells (translates being the result of a translation). In other words, all

combinations of translations (na, mb, kc) where $|n|$, $|m|$, and $|k|$ are less than or equal to 2 were generated for the reference molecule and its equivalents. For each atom an intermolecular radius was then assigned; the values were taken from Bondi.[56] For each atom in the reference molecule, distances to each atom in one of the generated molecules were calculated. If the interatomic distance for any such atom pair was found to be less than $1.5R_{ij}$, R_{ij} being the appropriate intermolecular radius sum, the two corresponding molecules were considered to be in contact. The process was repeated until the list of generated molecules was exhausted.

Interactions of the reference molecule with symmetry-inequivalent neighbors were found in a similar manner. In this case, if the reference molecule was A, molecule B and all its symmetry equivalents and translates were generated in the procedure.

Deuterium NMR spectra were obtained with a Bruker CXP-100 spectrometer equipped with a Bruker Aspect 3000 computer operating with a home-built probe in a narrow-bore magnet at 41.45 MHz. The sample diameter was 7 mm.

The measured NMR signals were the second half of the quadrupole echo formed by two 90° pulses. The width of a 90° pulse was 3.2 μs; the pulse separation was 30 μs unless otherwise noted. The data in the time domain were offset before Fourier transformation to put the echo maximum exactly at the first data point. Exponential weighting equivalent to 1000 Hz of line broadening was used. Each spectrum contained 2K data points and spanned 1.67 MHz. For measurements of peak positions the number of data points was expanded to 8K to give digital resolution of 407 Hz. The recorded positions were rounded off to the nearest multiple of 500 Hz.

Partially relaxed spectra were obtained by transformation of the second half of the quadrupole spin echo formed with a two-pulse sequence after partial recovery of the spin system from a saturating pulse train. Spin–lattice relaxation times were found by computer fit of the decay of the intensity of the highest point in the echo with time. In general, best results were obtained with a sum of two-exponential functions. The errors reported for the spin–lattice relaxation times are standard deviations determined by the program SAS (a statistical package available on the mainframe IBM 3040).

The temperature controller was calibrated against a thermocouple placed in a dummy sample. Baffles controlling the flow of gas within the probe were arranged so that the temperature of the sample was within 1 °C of the nominal temperature.

Spectral simulations were made with programs written in PASCAL and compiled on the Aspect 3000 computer on the spectrometer. Powder spectra were calculated by sampling all possible orientations of the magnetic field relative to the molecule (or pairs of molecular orientations interchanged by motion). The azimuthal angle was incremented in 1° steps; the steps in the longitudinal angle were scaled to the sine of the azimuthal angle times the azimuthal step. The spectra were corrected for the effect of finite pulse power,[57] but the effect of motion during the pulses was ignored.[58] The spectra were convoluted with a Lorentzian line shape having a width at half-height of 3000 Hz.

Calculations of relaxation times were based on the formulas of Torchia and Szabo[59] with details as explained in the text. Each orientation component of the simulated spectra was weighted to account for the degree to which the corresponding spectral component recovered from the saturating pulse train in the time allotted.

Results

Crystal Structure of the Mobile Form. Atomic positional parameters are given in Table II. Bond distances and angles are given in Tables III and IV. The molecular structures are shown with atomic labeling for both types of molecules present in the crystal molecules in Figures 1 and 2.

Deuterium NMR Spectroscopy of the Immobile Form. The immobile crystal modification of I with deuteriated inner rings gave the deuterium spectrum shown in Figure 3a at room temperature. The delay time between scans during accumulation of the spectrum was 100 s. Because at room temperature the spin–lattice relaxation time was estimated to be 3 min, the magnetization only partially recovered between scans for the spectrum shown. A spectrum calculated on the assumption of no reorientational motion matched the experimental spectrum reasonably well (Figure 3b).

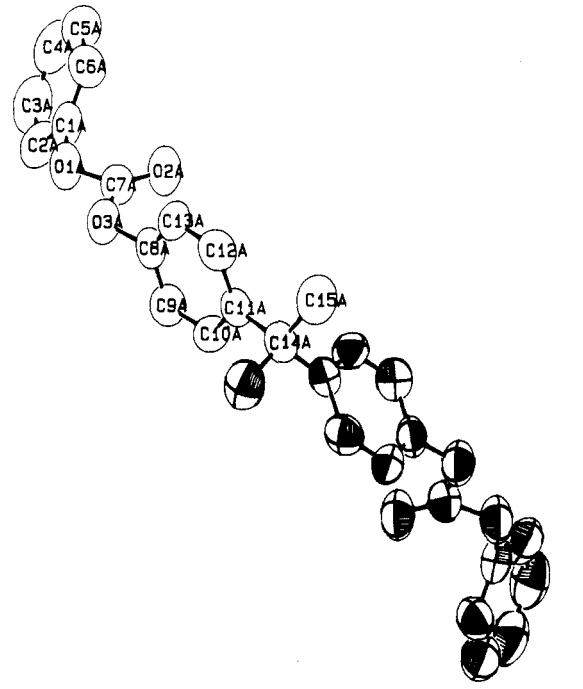

Figure 1. Plot of the A molecules viewed down the 2-fold axis. One half shows the atomic labeling, and the other half shows the thermal ellipsoids drawn at the 50% thermal probability level.

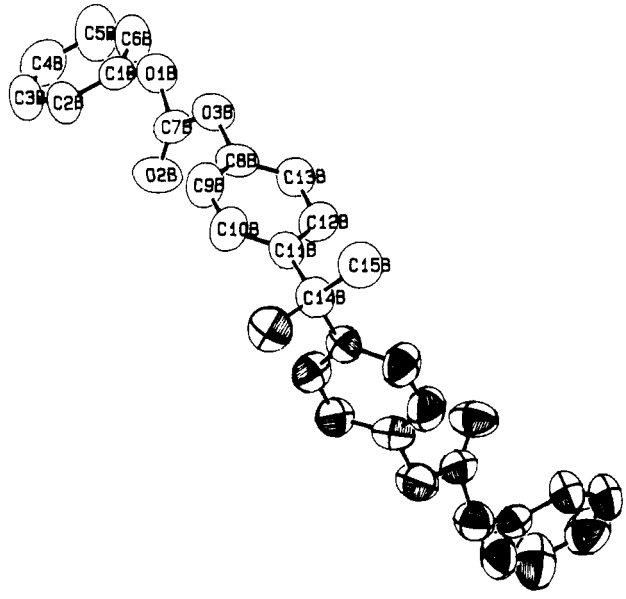

Figure 2. Plot of the B molecules viewed down the 2-fold axis.

Deuterium Nuclear Relaxation of the Mobile Form with Deuteriated Inner Rings. Observed recovery curves for the nuclear magnetization following saturation at 305, 325, and 350 K were best fit with a sum of two-exponential functions. The two relaxation times and the apparent weight of each component in the decay curves are given in Table V.

Deuterium NMR Spectra of the Mobile Form with Deuteriated Inner Rings. The two relaxation times observed differ at each temperature by almost 2 orders of magnitude. This relaxation time disparity allowed separation of the individual spectra associated with the fast-relaxing and slow-relaxing deuterium nuclei.

Table II
Positional Parameters (Esd's) for the Mobile Form

atom	x	y	z	B (A2)
O1A	0.3201 (2)	0.000	0.1944 (4)	7.7 (2)
O2A	0.3955 (2)	0.024 (1)	0.2026 (4)	8.1 (2)
O3A	0.3544 (2)	0.230 (1)	0.2908 (4)	7.7 (2)
C1A	0.3169 (2)	−0.162 (1)	0.1244 (6)	5.8 (2)
C2A	0.2977 (3)	−0.333 (2)	0.1573 (7)	8.2 (3)
C3A	0.2892 (3)	−0.494 (2)	0.0902 (8)	9.3 (3)
C4A	0.3000 (3)	−0.482 (2)	−0.0102 (8)	10.1 (3)
C5A	0.3191 (3)	−0.304 (2)	−0.0423 (7)	9.2 (3)
C6A	0.3270 (3)	−0.146 (2)	0.0250 (6)	7.5 (2)
C7A	0.3612 (2)	0.079 (2)	0.2262 (6)	6.5 (2)
C8A	0.3925 (2)	0.339 (1)	0.3367 (6)	5.9 (2)
C9A	0.4112 (2)	0.281 (1)	0.4347 (6)	5.7 (2)
C10A	0.4466 (2)	0.395 (1)	0.4841 (6)	5.7 (2)
C11A	0.4631 (2)	0.562 (1)	0.4389 (5)	4.5 (2)
C12A	0.4433 (3)	0.609 (1)	0.3402 (6)	6.8 (2)
C13A	0.4077 (2)	0.499 (2)	0.2892 (6)	7.4 (2)
C14A	0.500	0.693 (2)	0.500	5.6 (3)
C15A	0.5235 (3)	0.828 (1)	0.4276 (7)	8.2 (2)
O1B	0.1410 (2)	0.465 (1)	0.3872 (4)	6.9 (1)
O2B	0.1309 (2)	0.501 (1)	0.2116 (4)	8.1 (2)
O3B	0.0944 (2)	0.685 (1)	0.3198 (4)	7.2 (1)
C1B	0.1717 (2)	0.303 (1)	0.3874 (5)	5.6 (2)
C2B	0.2087 (2)	0.313 (2)	0.3381 (6)	7.8 (3)
C3B	0.2382 (3)	0.143 (2)	0.3469 (7)	8.9 (3)
C4B	0.2283 (3)	−0.020 (2)	0.4060 (7)	9.6 (3)
C5B	0.1913 (3)	−0.018 (2)	0.4568 (8)	9.9 (3)
C6B	0.1629 (3)	0.143 (2)	0.4472 (7)	7.9 (3)
C7B	0.1239 (2)	0.542 (1)	0.2943 (5)	5.5 (2)
C8B	0.0717 (3)	0.804 (1)	0.2365 (5)	5.9 (2)
C9B	0.0941 (3)	0.950 (2)	0.1939 (6)	8.1 (3)
C10B	0.0720 (3)	1.074 (2)	0.1182 (6)	7.4 (2)
C11B	0.0263 (2)	1.046 (1)	0.0821 (5)	5.3 (2)
C13B	0.0263 (2)	0.772 (1)	0.2080 (6)	6.1 (2)
C14B	0.000	1.178 (2)	0.000	5.4 (3)
C15B	−0.0311 (3)	1.319 (1)	0.0548 (6)	7.7 (2)
H2A	0.290	−0.344	0.227	8.3[a]
H3A	0.276	−0.617	0.110	9.9[a]
H4A	0.294	−0.590	−0.059	11.0[a]
H5A	0.328	−0.292	−0.111	9.1[a]
H6A	0.340	−0.023	0.004	7.9[a]
H9A	0.400	0.165	0.467	5.7[a]
H10A	0.460	0.357	0.552	5.9[a]
H12A	0.454	0.723	0.306	6.4[a]
H13A	0.394	0.536	0.221	7.5[a]
H15A1	0.546	0.906	0.468	7.9[a]
H15A2	0.537	0.744	0.381	7.9[a]
H15A3	0.502	0.915	0.389	7.9[a]
H2B	0.215	0.431	0.300	8.8[a]
H3B	0.264	0.140	0.312	8.6[a]
H4B	0.248	−0.134	0.413	9.5[a]
H5B	0.185	−0.132	0.497	10.4[a]
H6B	0.137	0.147	0.483	7.5[a]
H9B	0.125	0.971	0.217	8.3[a]
H10B	0.088	1.178	0.088	7.5[a]
H12B	−0.026	0.873	0.107	6.6[a]
H13B	0.010	0.670	0.240	6.4[a]
H15B1	−0.048	1.405	0.005	7.5[a]
H15B2	−0.051	1.239	0.089	7.5[a]
H15B3	−0.013	1.401	0.105	7.5[a]

[a] Atoms were allowed to ride on the parent carbons. Anisotropically refined atoms are given in the form of the isotropic equivalent displacement parameters defined as $^4/_3[a2\cdot B(1,1) + b2\cdot B(2,2) + c2\cdot B(3,3) + ab(\cos\gamma)\cdot B(1,2) + ac(\cos\beta)\cdot B(1,3) + bc(\cos\alpha)\cdot B(2,3)]$.

Table III
Bond Distances[a] (Esd's) for the Mobile Form

atoms		molecule A	molecule B
O1	C1	1.39 (1)	1.41 (1)
O1	C7	1.34 (1)	1.338 (9)
O2	C7	1.17 (1)	1.145 (9)
O3	C7	1.33 (1)	1.36 (1)
O3	C8	1.41 (1)	1.42 (1)
C1	C2	1.36 (1)	1.35 (1)
C1	C6	1.36 (1)	1.35 (1)
C2	C3	1.37 (2)	1.42 (2)
C3	C4	1.38 (1)	1.37 (2)
C4	C5	1.39 (2)	1.36 (1)
C5	C6	1.35 (1)	1.35 (1)
C8	C9	1.37 (1)	1.33 (1)
C8	C13	1.32 (1)	1.38 (1)
C9	C10	1.39 (1)	1.37 (1)
C10	C11	1.37 (1)	1.40 (1)
C11	C12	1.37 (1)	1.38 (1)
C11	C14	1.53 (1)	1.51 (1)
C12	C13	1.38 (1)	1.38 (1)
C14	C15	1.53 (1)	1.55 (1)

[a] Angstroms.

Table IV
Bond Angles[a] (Esd's) for the Mobile Form[b]

atoms	molecule A	molecule B
C1-O1-C7	118.4 (8)	117.5 (7)
C7-O3-C8	117.8 (7)	117.2 (7)
O1-C1-C2	115 (8)	122 (1)
O1-C1-C6	123 (1)	114.5 (8)
C2-C1-C6	121 (1)	123 (1)
C1-C2-C3	120 (1)	117 (1)
C2-C3-C4	120 (1)	119 (1)
C3-C4-C5	119 (1)	120 (1)
C4-C5-C6	120 (1)	120 (1)
C1-C6-C5	120 (1)	120 (1)
O1-C7-O2	127 (1)	130 (1)
O1-C7-O3	105.8 (8)	103.3 (8)
O2-C7-O3	127.3 (9)	126.3 (9)
O3-C8-C9	116.8 (9)	119.4 (9)
O3-C8-C13	121.3 (9)	118.4 (9)
C9-C8-C13	121.8 (9)	122.1 (9)
C8-C9-C10	117.7 (8)	120.2 (9)
C9-C10-C11	122.7 (8)	121.1 (9)
C10-C11-C12	116.2 (8)	116.2 (8)
C10-C11-C14	120.6 (8)	123.7 (8)
C12-C11-C14	123.2 (8)	120.0 (8)
C11-C12-C13	122.5 (9)	123.3 (8)
C8-C13-C12	119.2 (9)	117.1 (8)
C11-C14-C11′	112 (1)	109 (1)
C11-C14-C15	111.8 (4)	108.4 (4)
C11-C14-C15′	106.4 (4)	112.1 (5)
C15-C14-C15′	109 (1)	106 (1)

[a] Degrees. [b] Primed atoms are those related by 2-fold symmetry.

Table V
Spin-Lattice Relaxation Times for the Mobile Form of I

temp, K	component 1 T_1, s	component 1 %	component 2 T_1, s	component 2 %
305	0.16 ± 0.02	35	15.5 ± 1.2	65
325	0.10 ± 0.01	59	7.8 ± 1.4	41
350	0.03 ± 0.01	82	2.7 ± 0.6	18

Following a saturating pulse train, only the magnetization of the fast-relaxing population recovered in 5 times the short relaxation time. The corresponding spectra of the fast species are shown in Figures 4b, 5b, and 6b. In 3–4 times the long relaxation time, the magnetizations of both the fast- and slow-relaxing components recovered; the spectra for almost full recovery are shown in Figures 4a, 5a, and 6a. The differences of the spectra taken with a long recovery time and the spectra taken with a short recovery time are the spectra of the slowly relaxing deuterium nuclei shown in Figures 4c, 5c, and 6c. The methods by which the simulated spectra shown in the figures are calculated is described in the Discussion.

The maxima in the spectrum taken with a long recovery time at 305 K (Figure 2b) are at ±63 500 Hz, the same positions within the error of measurement as for the immobile form (Figure 1). The peak maxima in the spectrum

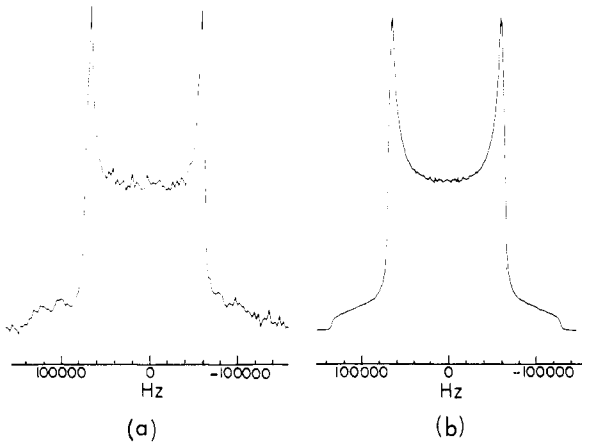

Figure 3. Experimental (a) and simulated (b) spectra of the immobile form of I with deuteriated inner rings at room temperature. A relaxation period of 100 s was used for the experimental spectrum.

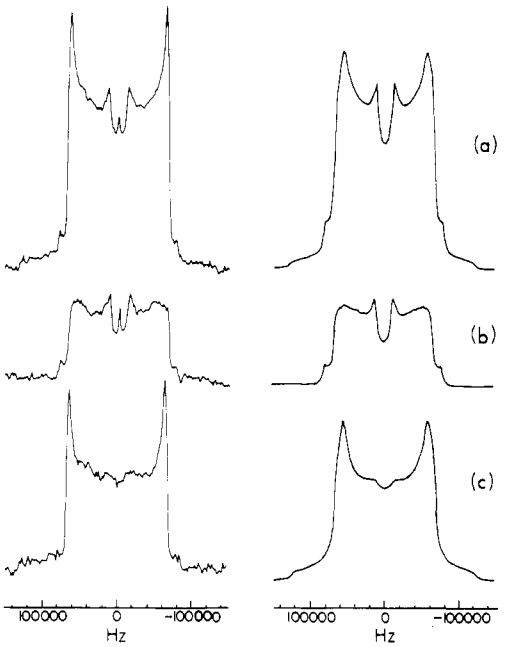

Figure 4. Experimental (left) and simulated (right) spectra of the mobile form of I with deuteriated inner rings for a sample temperature of 305 K. The periods for magnetization recovery following a saturating pulse train were (a) 50.0 s and (b) 0.75 s. The difference between (b) and (a) is shown in (c). The sharp experimental peaks at zero frequency are artifacts.

taken at 350 K (Figure 4b) are at ±13 000 Hz.

Another source of information about the rate and geometrical features of reorientational motion is the dependence of the spectrum on the time allowed for echo formation (the time between pulses in the two-pulse sequence).[60] At 305, 325, and 350 K, spectra of the mobile form of I were recorded for delay times of 30, 60, and 100 μs following a relaxation period of 10 s. These are shown in Figures 7–9.

Deuterium Nuclear Relaxation of I with Deuteriated Outer Rings. At 305 K recovery from a saturating pulse train was best fit by a sum of two exponentials with time constants of 0.06 ± 0.04 and 1.17 ± 0.16 s and weights of 0.21 ± 0.06 and 0.79 ± 0.06. At 350 K the time constants were 0.05 ± 0.01 and 0.20 ± 0.09 s, and the weights were 0.64 ± 0.22 and 0.36 ± 0.21.

Deuterium NMR Spectra of I with Deuteriated Outer Rings. The relaxation times of the slow and fast species in the end-deuteriated compound do not differ

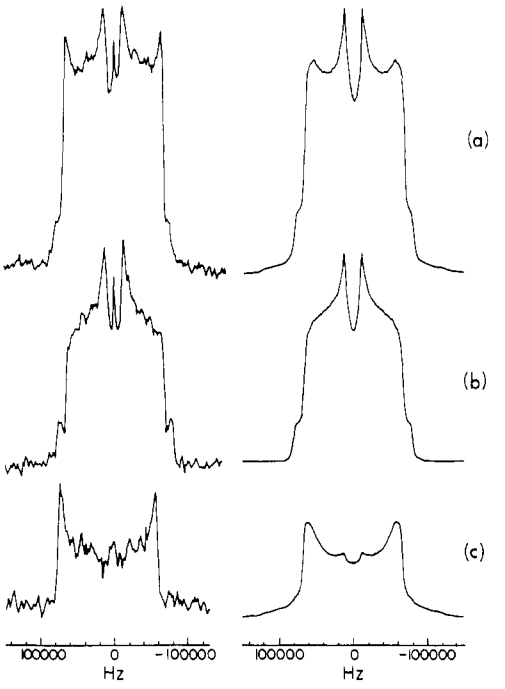

Figure 5. Experimental (left) and simulated (right) spectra of the mobile form of I with deuteriated inner rings for a sample temperature of 325 K. The periods for magnetization recovery following a saturating pulse train were (a) 30.0 s and (b) 0.5 s. The difference between (b) and (a) is shown in (c). The sharp experimental peaks at zero frequency are artifacts.

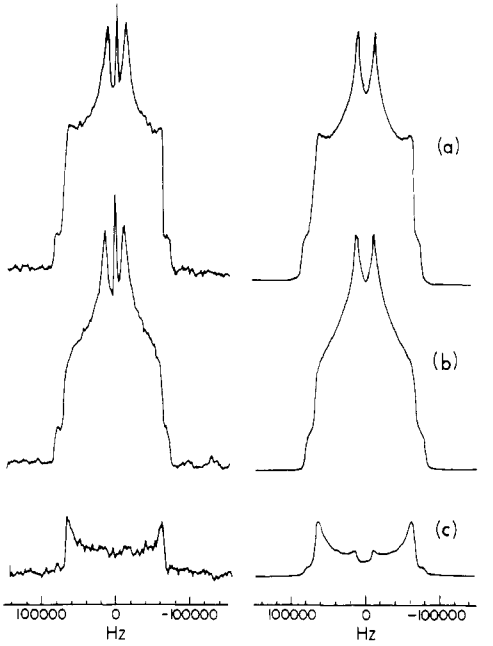

Figure 6. Experimental (left) and simulated (right) spectra of the mobile form of I with deuteriated inner rings for a sample temperature of 350 K. The periods for magnetization recovery following a saturating pulse train were (a) 10.0 s and (b) 0.15 s. The difference between (b) and (a) is shown in (c). The sharp experimental peaks at zero frequency are artifacts.

sufficiently for a clean separation of the spectra. Spectra taken at 305 and 350 K with delays for relaxation of 5 times the longer nuclear relaxation time are shown in Figure 10. The peak maxima at 350 K occur at ±15 000 Hz.

Deuterium NMR Spectroscopy of Deuteriated Bisphenol-A Polycarbonate. Spectra for ring-deuteriated BPAPC obtained at various temperatures almost perfectly matched those in the literature.[33–35] An impor-

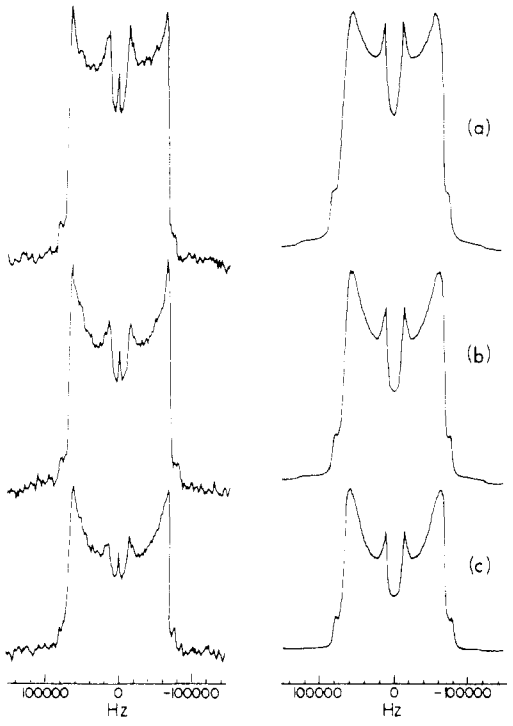

Figure 7. Experimental (left) and simulated (right) spectra of the mobile form of I with deuteriated inner rings for a sample temperature of 305 K for separations between the echo-forming pulses of (a) 30, (b) 60, and (c) 100 μs. A constant delay for magnetization recovery following a saturating pulse train of 10 s was used. The sharp experimental peaks at zero frequency are artifacts.

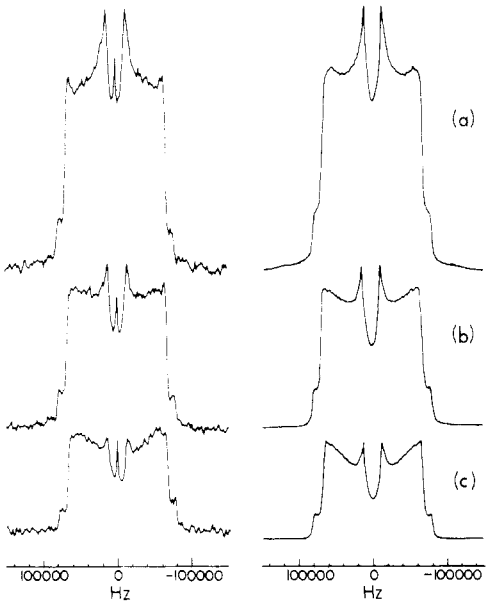

Figure 8. Experimental (left) and simulated (right) spectra for the mobile form of I with deuteriated inner rings for a sample temperature of 325 K and other conditions indicated in Figure 7. The sharp experimental peaks at zero frequency are artifacts.

tant feature linking the spectra of the polymer and those of the model compound is that the spectral maxima in the room-temperature spectrum of polycarbonate occur at the same frequency (±13 000 Hz) as do the maxima in the spectrum of the mobile form of I.

Discussion

Spectral Analysis and Simulation: Immobile Form of I with Deuteriation in the Inner Rings. One of the principal components of the quadrupole tensor must have

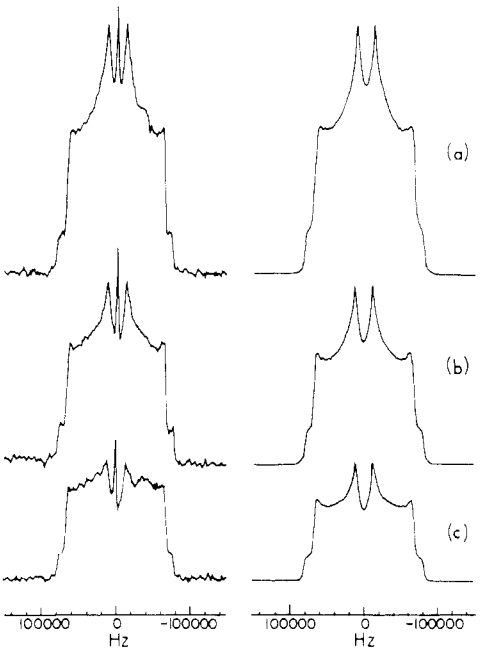

Figure 9. Experimental (left) and simulated (right) spectra for the mobile form of I with deuteriated inner rings for a sample temperature of 350 K and other conditions indicated in Figure 7. The sharp experimental peaks at zero frequency are artifacts.

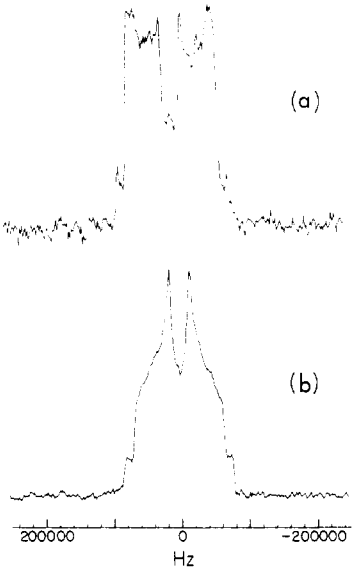

Figure 10. Experimental spectra of the mobile form of I with deuteriated end rings for sample temperatures of (a) 305 K and (b) 350 K. Delays following a saturating pulse train before data accumulation were (a) 6.0 s and (b) 1.0 s.

an angular frequency of $-2\pi(63500)$ rad/s, corresponding to the frequencies of the maxima in the spectrum in Figure 1. The edges of the spectrum were best fit if the other elements were taken to have values of $-2\pi(68000)$ and $2\pi(131500)$ rad/s. The local environment about an aromatic deuteron certainly is not exactly axially symmetric, but the assumption of asymmetry in the interaction tensor is largely a cosmetic convenience. The analysis of the spectra in terms of molecular motion to be described later leads to the same conclusions whether an axially symmetric or asymmetric interaction is assumed. The principal elements that were used correspond to e^2qQ/h = 175 333 Hz and η = 0.034.

The absorption frequencies of the inner-ring deuteron in I are ±131 500 Hz when the C–D bond is parallel to the magnetic field. We tentatively assign the z axis of the

principal axis system to the C–D bond direction. The x axis lies along the perpendicular to the aromatic ring, and the y axis is in the plane of the ring perpendicular to the C–D bond. The frequencies associated with the x and y directions were determined from the results for the mobile form of I (below).

Spectral Analysis: Mobile Form of I with Deuteriation in the Inner Rings. The deuterium spectrum of BPAPC is strongly influenced by 180° flipping of the aromatic rings.[33-36] The spectral changes with temperature observed for I also result largely from ring flipping.

For the orientation assumed for the quadrupolar tensor, ring flipping leaves the x principal element unchanged but mixes the y and z elements. For very fast flipping the quadrupole interaction is described by an effective interaction tensor having principal elements related to the original elements by

$$\omega_{yy}' = \omega_{yy} \cos^2 \phi + \omega_{zz} \sin^2 \phi$$
$$\omega_{zz}' = \omega_{yy} \sin^2 \phi + \omega_{zz} \cos^2 \phi \quad (1)$$

where ϕ is the angle between the C–D bond and the axis of rotation. The z axis of the motionally averaged tensor lies along the flipping axis.

Equations 1 give values for $\omega_{yy}/2\pi$ and $\omega_{zz}/2\pi$ of −14 750 and 82 750 Hz if we assume $\omega_{xx}/2\pi$ = −68 000 Hz. The value of ω_{yy} is too large to match the experimental value of −13 000 Hz. Examination of the experimental spectrum also suggests that the other averaged values are too large. Some motion in addition to ring flipping apparently takes place. Determination of the way in which the quadrupole coupling tensor must be averaged by this second process to account for the experimental results is elucidating. To discover what kind of averaging is needed, we work backward from the spectrum averaged by both processes shown in Figure 6b.

Initially we must find the effective time-averaged tensor that describes the averaged experimental spectrum. The value of one of the principal elements of this tensor can be found from the position of the maxima in the spectrum. We let this element be $\omega_{yy}/2\pi$ = −13 000 Hz. The values of the other two averaged elements must be determined from the spectral edges in Figure 6b. The positions of the spectral edges are more difficult to establish than is the position of the spectral maxima, but reasonable choices for the other tensor elements are $\omega_{xx}/2\pi$ = −65 000 Hz and $\omega_{zz}/2\pi$ = 78 000 Hz, where we have taken into account that $\omega_{xx} + \omega_{yy} + \omega_{zz} = 0$.

We now work backward with eq 1 to eliminate the averaging effect of ring flipping and to give us the elements of an effective tensor reflecting the averaging of the secondary process alone. The tensor elements are $\omega_{yy}/2\pi$ = −58 500 Hz and $\omega_{zz}/2\pi$ = 123 500 Hz; $\omega_{xx}/2\pi$ is still −65 000 Hz. The degree to which these elements are less than the corresponding values of −63 500, 131 500, and −68 000 Hz found for the rigid tensor reflects the averaging effect of the secondary process on the tensor.

The spectrum in Figure 6b could allow slightly larger values of ω_{xx} and ω_{zz} than were used for the above calculation. A choice of $\omega_{xx}/2\pi$ = −70 000 Hz and $\omega_{zz}/2\pi$ = 83 000 Hz leads to $\omega_{yy}/2\pi$ = −56 000, $\omega_{zz}/2\pi$ = 131 000 Hz, and $\omega_{xx}/2\pi$ = −70 000 Hz for the elements of the partially averaged tensor. In this case ω_{xx} would actually have to be increased by the secondary averaging. Other alternative choices of the spectral parameters also lead to unreasonable values for the elements of the partially averaged tensor.

We will accept at this point the values first chosen as the most reasonable choices. The secondary process appears to average ω_{yy} and ω_{zz} together while having a smaller effect on ω_{xx}.

Alignment of the z axis at an angle other than 60° with respect to the flipping axis could explain the spectral frequencies without the need for a secondary averaging process. Simple calculations with eq 1 show that a deviation in the plane of the ring as small as 1° would be sufficient to account for the reduced values of ω_{yy} and ω_{zz}. However, analysis of the orientation dependence of spin–lattice relaxation caused by ring flipping shows that a secondary process in addition to ring flipping is nevertheless required by the data. For the ring-flipping rate giving the best overall fit to the spectrum shown in Figure 4b, more than 25% of the nuclei would have a spin–lattice relaxation time greater than 0.5 s if no other process were involved. Because only 0.75 s was allowed for recovery of the spin system from saturation, the signal from the slowly relaxing portion of the sample would be severely attenuated. Indeed the spectrum was only roughly approximated in terms of ring flipping alone. A secondary process that makes the overall motion more isotropic is needed for a good fit of the experimental result.

Both low-amplitude motion about the same axis as ring flipping (ring oscillation) or motion about an axis perpendicular to the aromatic ring (ring wiggling) would lead to more isotropic spin–lattice relaxation than does ring flipping alone. Our data do not cleanly differentiate between these two types of secondary processes. Because motion about an axis perpendicular to the ring comes closest to accounting for the observed spectral frequencies, we have chosen to calculate simulated spectra in terms of that process. The actual secondary process accompanying ring flipping both in the model compound and in BPAPC probably is not purely ring flipping or ring wiggling.

We now need to know how large the ring wiggling must be to account for the averaging of the quadrupole tensor actually observed for I. For simplicity we approximate the wiggling as a two-site jump between positions separated by a rotational angle about the perpendicular axis of 2ϕ. Equations having the same form as eq 1 are appropriate to account for the averaging of the tensor elements if ϕ is taken as half the jump angle. If the original tensor elements have values $\omega_{xx}/2\pi$ = −68 000 Hz, $\omega_{yy}/2\pi$ = −63 500 Hz, and $\omega_{zz}/2\pi$ = 131 500 Hz, the elements of the tensor averaged by wiggling are $\omega_{xx}/2\pi$ = −68 000 Hz, $\omega_{yy}/2\pi$ = −58 728 Hz, and $\omega_{zz}/2\pi$ = 126 728 Hz for ϕ = 9°. Ring flipping reduces the values to −68 000, −12 364, and 80 364 Hz, in reasonable agreement with the observed values of −65 000, −13 000, and 78 000 Hz. The total overall angle of rotation thus appears to be close to 20°. The discrepancies between the calculated and observed values probably result from the fact that the secondary process is not purely a rotation about the vertical axis and from the imprecise knowledge of the orientation of the PAS. The actual amplitude of the motion may be somewhat less than 20°.

Spectra Simulation: Mobile Form of I. The calculation of simulated spectra was designed to incorporate the salient features of the motional model outlined above without leading to unwieldy computer programs. The simplifications used in simulation inevitably lead, of course, to imperfections in the fit of the spectra. Nevertheless, most features of the experimental results are reproduced quite well, including the effect of spin–lattice nuclear relaxation.

The wiggling motion was modeled by a jump between sites separated by a 20° angle of rotation about the perpendicular axis. Motion of this amplitude affects the ob-

Table VI
Rate Constants (s^{-1}) Used in Simulations

	slow rate		fast rate	
temp, K	flipping	oscillation	flipping	oscillation
305	9.0×10^3	5.4×10^7	1.0×10^6	6.0×10^6
325	2.15×10^4	1.075×10^5	2.4×10^6	7.2×10^6
350	6.0×10^4	3.0×10^5	9.0×10^6	2.7×10^7

served spectral line shape only slightly (although not negligibly). For the purposes of calculation of line shapes, the wiggling was assumed to be fast at all temperatures. The elements of the effective quadrupole tensor were simply reduced in magnitude accordingly. This approximation noticeably, but not severely, interferes with matching of the spectra for slow ring flipping.

Even motions of small amplitude may contribute strongly to spin–lattice relaxation. Therefore, the rate of spin–lattice relaxation associated with wiggling was calculated explicitly (with the full quadrupole tensor) and added to the rate of spin–lattice relaxation associated with ring flipping (calculated with the reduced tensor). The rate of the jump was assumed to be faster than the rate of ring flipping by a factor that was an input parameter to the computer program.

In a fully rigorous calculation the effect on relaxation of the two motions acting together would have to be determined. Preaveraging of the tensor used in the calculation of relaxation by ring flipping would not be assumed. Again, the errors introduced by the approximation are not believed to be important.

Table VI lists the motional parameters giving the best overall fit to the experimental observations. In those cases for which there was significant motional averaging of the spectra, the rates of ring flipping were chosen to give the best overall line shapes. The rate of ring wiggling was then chosen to be a multiple of the rate of ring flipping such that the average relaxation rate matched the experimental value of ring flipping. When there was very little motional averaging of the spectra, rate constants were chosen to give the best calculated relaxation times. The spectra in Figures 7–9 were simple calculated with the parameters already found from the other spectra and relaxation parameters.

The worst discrepancies between the calculated and experimental spectra occur for slow rates of ring flipping. As noted above, it is for slow ring flipping that the failure to account fully for spectral averaging by ring wiggling should be most important.

The effect of changes in pulse separation is also imperfectly simulated although the basic changes in the shape of the experimental spectra as the pulse separation is increased do show up in the calculations (Figures 7–9).

The apparent shift in the populations of rings flipping relatively rapidly and those flipping slowly comes about because a portion of the signal from each population is lost during the formation of the echo. There is no real shift in the two populations. The loss is greater for that population whose ring-flipping rate is comparable to the inverse of the pulse separation. At 305 K the signal from the faster population is lost preferentially; at 350 K the signal from the slower population is lost preferentially. The calculations reproduce this aspect of the results very nicely.

In total, the calculated spectra provide a reasonable match to the experimental spectra. No serious problems with a combination of ring flipping with ring wiggling show up.

Detailed Molecular Model for the Motion. Numerous calculations have shown that the methyl groups in BPAPC provide little hindrance to rotation of the phenyl rings adjacent to them,[44,47,62–65] particularly if the rings are assumed to move in a cooperative fashion. Therefore, we will focus on the interactions of the phenyl rings with the carbonate group as the factor controlling the nature of chain motion. Let us first understand the lowest energy conformation of the molecule in this region.

In the immobile crystalline form the two ends of I are inequivalent. In the mobile form there are two types of molecules, each with an axis of symmetry. These are shown in Figures 1 and 2. All together, we know the molecular conformation around the carbonate group in four different local environments. In each of these the carbonate group is in the trans–trans conformation.

The angles between the two types of carbonate groups and the central phenyl rings in the immobile crystal have magnitudes of 89.2° and 89.0°. The corresponding angles in the mobile crystals are 84.3° and 75.2°. The angles between the carbonate group and the outer rings are 48.0° and 77.6° in the immobile form and 57.6° and 53.4° in the mobile form.

The perpendicular orientation of the carbonate group relative to the inner phenyl rings appears to be most favorable for I. Some deviation of the outer phenyl rings from the perpendicular orientation does occur, but these rings are dissimilar from those in the polymer in that they are tied down at one end only.

Let us now examine the effect of rotation of the bisphenol-A rings in I while the rest of the molecule is held in the conformation described above. Ultimately, unaccompanied rotation of the rings leads to a locally planar form in which the ortho ring hydrogen interacts strongly with the carbonyl oxygen. The increase in energy resulting from steric crowding is partially offset by the conjugation of the ring with the carbonate group in the planar form, but clearly the steric effect is more important than the electronic effect in determining the overall conformational energy. Otherwise, the local ground-state conformation would be locally planar.

Previous calculations for BPAPC have indicated that the planar local conformation sits at an energy maximum.[61–64] Estimates of the height of the maximum have varied from about 1 kcal/mol to more than 20 kcal/mol, however. The discrepancies arise because of differences in the choice of the parameters to describe the steric and conjugative interactions. Regardless of how unstable the planar form actually is, it will not serve as the transition state for ring flipping if another, lower energy transition state is easily accessible to the molecule.[65]

Examination of molecular models suggests that there are, indeed, other possibilities for the transition state to ring flipping. Simultaneous rotation through an angle of perhaps 20° about the O_3–C_7 and O_1–C_1 bonds can take place with minor overall changes in the conformation of the molecule as a whole and moves the carbonyl group away from the adjacent inner phenyl ring such that the closest approach of the ortho hydrogen and the carbonyl oxygen is considerably greater than it is in the planar form. Thus distortion of the carbonate unit from the planar trans–trans conformation facilitates ring flipping. Carbonate movement is tied to longer range motion of the phenyl rings and the methyl groups.

Different experimental methods simply pick up different aspects of the overall molecular motion. Dielectric relaxation is sensitive to the carbonyl motion itself; dynamic mechanical spectroscopy detects motion of the chain as a whole; NMR spectroscopy is sensitive to both ring flipping and ring oscillation.

Effectively, the carbonyl group in both I and BPAPC acts as a turnstile with respect to ring motion. In the most stable conformation the turnstile is closed, and the ring cannot move. When the carbonate group becomes distorted, the turnstile opens up and ring flipping can take place. Note that movement of the carbonyl group probably requires coordinated motions in neighboring molecules so that lattice motions may also be a part of the overall process.

In principle, motion of the carbonyl group itself could be detected in the ^{13}C NMR spectrum of the carbonyl group. In practice, the spectrum of ^{13}C-labeled BPAPC is almost temperature independent.[41] This might be taken as a contraindication of carbonyl motion. The elements of the chemical-shift tensor that correspond to orientation of the magnetic field along the CO bond and perpendicular to the face of the carbonyl group differ only slightly, however. Motion that partially averages these elements would have little effect on the NMR spectrum. This is exactly the kind of motion that we are now proposing. The temperature independence of the spectrum of the carbonyl carbon is actually an important piece of evidence in favor of the model presented.

Motion of the End Rings in I. As might be expected, the end rings on I are more mobile than are the inner rings, as evidenced by shorter spin–lattice relaxation times for the deuterium nuclei on the end rings and by highly averaged spectra for these nuclei (Figure 10). The principal motion of the end rings, like that of the central rings of I, is, nevertheless, flipping. The details of motion for the end rings is less relevant to that for BPAPC than is that of the inner rings, and we have not attempted a detailed analysis.

Influence of Crystal Packing on Ring Flipping in I. An indispensable component of the proposed motional model for the mobile form of I is the presence of at least two distinct kinds of carbonate groups in the crystal such that the rate of ring flipping in the vicinity of one is facilitated relative to the other. In principle, the distinction could relate either to conformational differences or to differences in molecular packing in the crystal. Strictly speaking, the presence of two crystallographically independent molecules in the crystal guarantees that such differences exist. However, symmetry arguments do not provide an estimate of how significant the differences are. In fact, it is frequently observed that crystallographically independent molecules are related by an approximate (non-space group) symmetry element.[66] In such cases, symmetry independence results in a distinction without much importance.

The bond angles and the conformations of the two molecules in the mobile crystal are very similar (Tables II–IV). This would seem to weigh against a conformational explanation for the differences in the rates of ring flipping for the two. If structural evidence for a physical distinction between the two types of molecules exists, it must lie in the nature of the interactions of the two types of carbonyl groups with neighboring molecules. Accordingly, we have performed a detailed packing analysis of the mobile crystals. A number of significant A–A and B–B interactions between a reference molecule and its symmetry-related neighbors are summarized in Tables VII and VIII. The numbers of interactions between A and B molecules are counted in Table IX.

Examination of the tables suggests that the environment provided A by A neighbors is very similar to the environment provided B molecules by B neighbors. In each case, however, the translates along the crystallographic *b* direction account for most of the close interatomic contacts. The translation chain along the *b* direction for the A molecules is shown stereoscopically in Figure 11; that for the B molecules is displayed in Figure 12. As expected on the basis of the distance calculations, the interactions between A molecules is similar to that between B molecules. More importantly, the carbonyl groups in neither type of molecule are in close contact with atoms on neighboring like molecules. This point has been verified with a repeat of the calculations leading to Tables VII and VIII in which $1.05R_{ij}$ was used as the cutoff distance. Only molecules corresponding to the first two entries in Tables VII and VIII have contacts within the cutoff distance, and none of these involve the carbonyl groups.

Table IX shows that each molecule of type A contacts 10 molecules of type B. Likewise, each molecule of type B contacts 10 molecules of type A. Clearly molecules 7 and 8 in Table IX account for the largest number of A–B

Table VII
Intermolecular Contacts in the Mobile Form of I (Type A–A)[a]

molec no.	sym designation[b]	no. of contacts[c]
1	1(0,−1,0)	176
2	1(0,1,0)	176
3	2(−1,−1,−1)	39
4	2(−1,0,−1)	39
5	2(0,−1,1)	39
6	2(0,0,1)	39

[a] Both the reference molecule and the neighboring molecules are type A. [b] In the calculations a full molecule was generated from the coordinates of the half molecule (Table II) by application of the appropriate crystallographic diad. This approach gives only two symmetry operations in space group *C*2 for consideration, namely, the identity operation and the centering operation. In the symmetry designations given above, the number outside the parentheses refers to the symmetry operation and the three numbers inside the parentheses refer to lattice translations for which $1 = x, y, z$; $2 = x + {}^1/_2, y + {}^1/_2, z$. [c] The number of close interatomic distances between the reference molecule and the molecule whose symmetry designation is given in the preceding column. Close is defined as $r_{ij} < 1.5R_{ij}$, where r_{ij} is the observed distance and R_{ij} is the appropriate intermolecular radius sum.

Table VIII
Intermolecular Contacts in the Mobile Form of I (Type B–B)[a]

molec no.	sym designation[b]	no. of contacts[c]
1	1(0,−1,0)	180
2	1(0,1,0)	180
3	2(−1,−1,−1)	34
4	2(−1,0,−1)	34
5	2(0,−1,1)	34
6	2(0,0,1)	34

[a] Both the reference molecule and the neighboring molecules are type B. [b,c] See Table VII.

Table IX
Intermolecular Contacts in the Mobile Form of I (Type A–B)[a]

molec no.	sym designation[b]	no. of contacts[c]
1	1(0,−1,0)	15
2	1(1,−1,1)	15
3	1(0,0,0)	25
4	1(1,0,1)	25
5	2(0,−2,0)	40
6	2(0,−2,1)	40
7	2(0,−1,0)	135
8	2(0,−1,1)	135
9	2(0,0,0)	70
10	2(0,0,1)	70

[a] The reference molecule is type A, and the neighboring molecules are type B. [b,c] See Table VII.

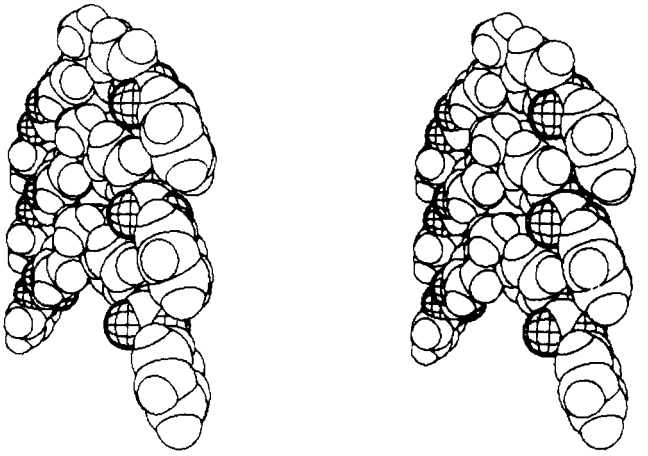

Figure 11. Stereoscopic view of the A molecules translated along the crystallographic *b* direction in the mobile form of I.

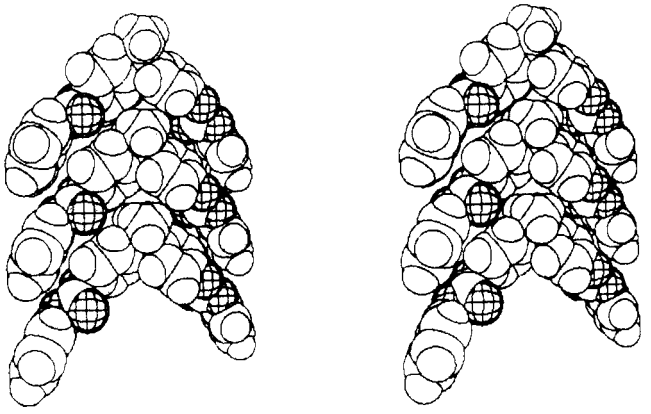

Figure 12. Stereoscopic view of the B molecules translated along the crystallographic *b* direction in the mobile form of I.

contacts. These B molecules along with the reference A molecule are depicted in Figure 13. In the figure, molecule A is in the center, and molecule B (numbers 7 and 8 in Table IX) are above and below it. Since the two B molecules are related by a translation along the crystallographic *c* axis (vertical in the figure), the figure contains 1.5 repeat units of an infinite chain. The central molecule must be translated ±1 time in the c direction to generate the next higher and the next lower members of the chain, respectively.

In the case of A–B interactions there appears to be a definite difference in the local environments of the carbonyl groups in each type of molecule. It is clear that none of the oxygen atoms in the central molecule is in close contact with atoms belonging to B molecules. On the other hand, the carbonyl oxygens of the bottom molecule (and of its translate, the top molecule) apparently touch the ring atoms of the central molecule or one of its not shown translates. This fact has been verified by distance calculations where we find that for each oxygen atom in molecule B there is at least one atom on molecule A (or one of its equivalents) for which the interatomic distance exceeds the appropriate intermolecular radius sum by less than 0.03 Å. In other words, each carbonyl oxygen of molecule B is within 0.03 Å of some atom on molecule A or one of its equivalents. The arrangement is not reciprocal; no carbonyl oxygen in molecule A is close to an atom in molecule B.

The distance calculations suggest that intermolecular interactions involving the carbonyl groups may be the source of the observed differences in the rate of ring flipping for the A and B molecules. In the context of the proposed motional model, we would identify the molecules with the tightly packed carbonyl groups (the B molecules) as those having slowly flipping rings. Further evidence to support this conclusion could be obtained by attempting to calculate the "in-crystal" rates of ring flips (or the associated activation energies) for molecules A and B with the atom–atom potential method. This type of calculation has been used as a means of exploring the reorientation of rigid molecules in crystals.[67] At least two types of lattice dynamical models can be used. In the most straightforward approach, one allows the reference molecule to reorient (typically about one of the inertial axes) while keeping all other molecules in the crystal in the equilibrium orientation. In the second approach, the first and second coordination shells of the reference molecule are allowed some libration as an approximation to the motion expected of a lattice phonon. The second model has been more successful than the first in reproducing observed activation barriers. The present case is much more complicated than those treated previously because coupled intermolecular motions probably must be considered along with the intramolecular motions. Each internal motion would have associated with it an inherent torsional barrier as well as whatever barriers are imposed by adjacent molecules in the crystal. Such a calculation is outside the scope of this work. Hence, the qualitative notion that the carbonyl groups in molecule A are significantly less restricted by intermolecular interactions than are those on molecule B is the best that can be offered at present.

Theoretically, analysis of the thermal-motion parameters obtained from X-ray diffraction can provide information about molecular motions in crystals.[74] Separation of rigid-body motion from non-rigid-body motions is nontrivial, however. We have not attempted such an analysis. The thermal ellipsoids shown in Figures 1 and 2 can encompass considerable internal motion of the carbonate groups and the aromatic rings.

Activation Parameters for Ring Flipping in I. Three temperature points provide a poor basis for determination of Arrhenius parameters. Nevertheless, use of eq 2 to calculate activation energies (E_a) and prefactors

$$k = k_0 \exp(-E_a/RT) \quad (2)$$

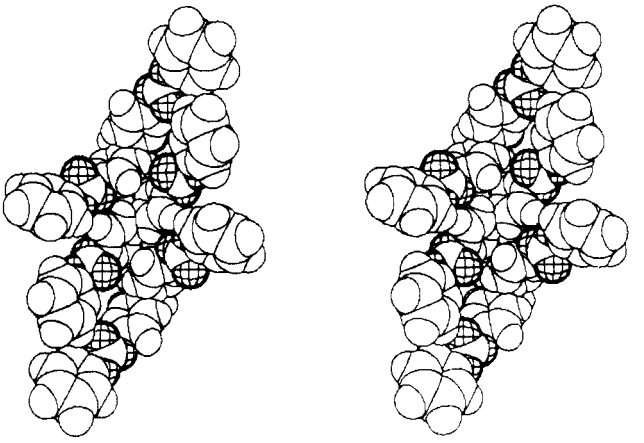

Figure 13. Stereoscopic view showing interactions of an A molecule (middle) with B molecules (top and bottom) in the mobile form of the model compound.

Table X
Arrhenius Parameters for Ring Flipping in I

temp interval	fast flip		slow flip	
	E_a, kcal/mol	k_0	E_a, kcal/mol	k_0
305–325 K	9.0	2.7×10^{12}	8.6	1.3×10^{10}
325–350	12.0	2.7×10^{14}	9.3	3.8×10^{10}

k_0 for fast and slow ring flipping is enlightening (Table X). The activation energies appear to be temperature dependent, especially for the faster process, so values were found for each pair of experimental temperatures. The apparent temperature dependence may be an artifact resulting from the use of data combined from an analysis of relaxation times and line shapes. Multiple routes by which the rings at each crystal site could flip could also lead to temperature-dependent activation energies, however.

In spite of the uncertainty in the activation parameters, it is interesting that the observed activation energies for ring flipping in the model compound are not much different from the value of 9.1 kcal/mol found for BPAPC.[36] Nevertheless, there is a clear variation of ring-flipping rates from site to site in the crystals.

A distribution of free volume in the amorphous polymer is sometimes invoked to explain the distribution of rates for ring flipping that occur in the polymer. Interestingly, the density of the mobile form calculated from the X-ray structure of I is 1.240 g/cm^3, whereas that of the immobile form is 1.308 g/cm^3. The density of the mobile form is thus well on the way toward that of amorphous BPAPC[68] (1.20 g/cm^3) from that of the immobile form. Recent work by Schaefer and co-workers shows that compression of BPAPC also hinders ring motion.[75] The density differences tell nothing about the specific interaction between adjacent molecules in the crystal structure that directly control motion, however.

The carbonate group plays a major role in the motional model for BPAPC that we have presented. Intermolecular interactions between the carbonyl group and the adjacent chains may very well be the factor determining the rate of ring flipping for any given chain segment. It is intriguing, therefore, that recent work was shown that dibutyl phthalate, which is known to act as an antiplasticizer in BPAPC in low concentrations, interacts specifically with the carbonate region of the molecule.[70] Antiplasticizers are known to suppress the secondary loss peaks of BPAPC in both dielectric and mechanical spectroscopy.[70-73]

In any case, the total spread of ring-flipping rates for I, which spans at least 3 orders of magnitude if the rates in both the mobile and immobile forms are taken into account, is consistent with the observation that the ring-flipping rates in BPAPC span several orders of magnitude.[36] The model compound provides hard evidence that packing alone can account for the rate distribution in the amorphous polymer.

Conclusions

Short-range motion in bisphenol-A polycarbonate is best interpreted as a cooperative motion involving both the carbonate group and the phenyl rings. Movement of the carbonyl group away from the phenyl rings enables 180° flips of those rings. The rate of ring flipping is strongly dependent upon the local environment of the phenyl rings and the carbonate group in crystalline I. This explains the broad distribution of ring-flipping rates that has been observed in amorphous BPAPC.

Acknowledgment. The help of Dr. Mridula Nair and Dr. David Teegarden in preparing the deuteriated forms of I was essential. John Tribone analyzed the crystalline forms of I with differential scanning calorimetry, Joe Caluorie provided X-ray diffraction data, and Tom Criswell did the mass spectrometry. Discussions with Dr. Dennis Massa and Dr. John Pochan were very beneficial.

Registry No. I, 20325-64-8; BPAPC (copolymer), 25037-45-0; BPAPC (SRU), 24936-68-3.

Supplementary Material Available: Tables of thermal parameters (2 pages) and structure factor amplitudes (25 pages) for the mobile crystal. Ordering information is given on any current masthead.

References and Notes

(1) Heijboer, J. *J. Polym. Sci., Part C* **1968**, *16*, 3755.
(2) Heijboer, J. *Ann. N.Y. Acad. Sci.* **1976**, *279*, 104.
(3) Boyer, R. F. *Polym. Eng. Sci.* **1968**, *8*, 161.
(4) Sacher, E. *J. Macromol. Sci., Phys.* **1974**, *B9*, 163.
(5) Sacher, E. *J. Macromol. Sci., Phys.* **1975**, *B11*, 403.
(6) Sacher, E. *J. Appl. Polym. Sci.* **1975**, *19*, 1421.
(7) Gerberich, W. W.; Martin, G. C. *J. Polym. Sci., Polym. Phys. Ed.* **1976**, *14*, 897.
(8) Mercier, J. P.; Aklonis, J. J.; Litt, M.; Tobolsky, A. V. *J. Appl. Polym. Sci.* **1965**, *9*, 447.
(9) Martin, G. C.; Gerberich, W. W. *J. Mater. Sci.* **1976**, *11*, 231.
(10) Wyzgoski, M. G.; Yeh, G. S. Y. *Int. J. Polym. Mater.* **1974**, *3*, 133.
(11) Legrand, D. G. *J. Appl. Polym. Sci.* **1969**, *13*, 2129.
(12) Wyzgoski, M. G.; Yeh, G. S. Y. *J. Macromol. Sci., Phys.* **1974**, *B10*, 441.
(13) Koyama, K.; Wada, E.; Nagata, Y.; Watanabe, Y.; Futamura, H. *Rep. Prog. Polym. Phys. Jpn.* **1972**, *15*, 317.
(14) Kastelic, J. R.; Baer, E. *J. Macromol. Sci., Phys.* **1973**, *B7*, 679.
(15) Litt, M. H.; Tobolsky, A. V. *J. Macromol. Sci., Phys.* **1967**, *B1*, 433.
(16) Robertson, R. E.; Patel, A. M. *Polym. Eng. Sci.* **1972**, *12*, 346.
(17) Bauwens-Crowet, C.; Bauwens, J. C.; Homes, G. *J. Mater. Sci.* **1972**, *7*, 176.
(18) Bauwens, J. C. *J. Mater. Sci.* **1972**, *7*, 577.
(19) Joseph, E. A.; Lorenz, M. D.; Barlow, J. W.; Paul, D. R. *Polymer* **1982**, *23*, 112.
(20) Sacher, E. *J. Macromol. Sci., Phys.* **1974**, *B10*, 319.
(21) Yee, A. F.; Smith, S. A. *Macromolecules* **1981**, *14*, 54.
(22) Matsuoka, S.; Ishida, Y. *J. Polym. Sci., Part C* **1966**, *14*, 247.
(23) Watts, D. C.; Perry, E. P. *Polymer* **1978**, *19*, 248.
(24) Garfield, L. J. *J. Polym. Sci., Part C* **1970**, *30*, 551.
(25) Vosskotter, G.; Kosfeld, R. *Kolloid Z. Z. Polym.* **1967**, *216*, 85.
(26) Davenport, R. A.; Manuel, A. J. *Polymer* **1977**, *18*, 557.
(27) Tekeley, P.; Turska, E. *J. Macromol. Sci., Phys.* **1978**, *B15*, 433.
(28) Stefan, D.; Williams, H. L. *J. Appl. Polym. Sci.* **1974**, *18*, 1451.
(29) Jones, A. A.; O'Gara, J. F.; Inglefield, P. T.; Bendler, J. T.; Yee, A. F.; Ngai, K. L. *Macromolecules* **1983**, *16*, 658.
(30) Steger, T. R.; Schaefer, J.; Stejskal, E. O.; McKay, R. A. *Macromolecules* **1980**, *13*, 1127.
(31) Schaefer, J.; Stejskal, E. O.; Buchdahl, R. *J. Macromol. Sci., Phys.* **1977**, *B13*, 665.
(32) Connoly, J. J.; Inglefield, P. T.; Jones, A. A. *J. Chem. Phys.* **1987**, *86*, 6602.
(33) Spiess, H. W. *J. Mol. Struct.* **1983**, *111*, 119.
(34) Spiess, H. W. *Colloid Polym. Sci.* **1983**, *261*, 193.
(35) Fischer, E. W.; Hellman, G. P.; Spiess, H. W.; Horth, F. J.; Ecarius, U.; Wehrle, M. *Macromol. Chem. Phys., Suppl.* **1985**, *No. 12*, 189.
(36) Schmidt, C.; Kuhn, K. J.; Spiess, H. W. *Prog. Colloid Polym. Sci.* **1985**, *71*, 71.
(37) Roy, A. K.; Jones, A. A.; Inglefield, P. T. *J. Magn. Reason.* **1985**, *64*, 441.
(38) Inglefield, P. T.; Amici, R. M.; O'Gara, J. F.; Hung, C.-C.; Jones, A. J. *Macromolecules* **1983**, *16*, 1552.
(39) O'Gara, J. F.; Jones, A. A.; Hung, C.-C.; Inglefield, P. T. *Macromolecules* **1985**, *18*, 1117.
(40) Roy, A. K.; Jones, A. A.; Inglefield, P. T. *Macromolecules* **1986**, *19*, 1356.
(41) Henrichs, P. M.; Linder, M.; Hewitt, J. M.; Massa, D.; Isaacson, H. V. *Macromolecules* **1984**, *17*, 2412.
(42) Schaefer, J.; Stejskal, E. O.; McKay, R. A.; Dixon, W. T. *Macromolecules* **1984**, *17*, 1479.
(43) Schaefer, J.; Stejskal, E. O.; Perchak, D.; Skolnik, J.; Yaris, R. *Macromolecules* **1985**, *18*, 368.
(44) Perchak, D.; Skolnick, J.; Yaris, R. *Macromolecules* **1987**, *20*, 121.
(45) Jones, A. A. *Macromolecules* **1985**, *18*, 902.
(46) Perez, S.; Scaringe, R. P. *Macromolecules* **1987**, *20*, 68.
(47) Henrichs, P. M.; Luss, H. *Macromolecules* **1988**, *21*, 860.
(48) Schaefer, J.; Sefcik, M. D.; Stejskal, E. O.; McKay, R. A.; Dixon, W. T.; Cais, R. E. *Macromolecules* **1984**, *17*, 1107.
(49) Cholli, A. L.; Dumais, J. J.; Engel, A. K.; Jelinski, L. W. *Macromolecules* **1984**, *17*, 2399.
(50) Rice, D. M.; Wittebort, R. J.; Griffin, R. G.; Meirovitch, E.; Stimson, E. R.; Meinwald, Y. C.; Freed, J. H.; Scheraga, H. A. *J. Am. Chem. Soc.* **1981**, *103*, 7707.

(51) McCammon, J. A.; Lee, C. Y.; Northrup, S. H. *J. Am. Chem. Soc.* **1983**, *105*, 2323.
(52) Rice, D. M.; Meinwald, Y. C.; Scheraga, H. A.; Griffin, R. G., personal communication.
(53) Gall, C. M.; DiVerdi, J. A.; Opella, S. J. *J. Am. Chem. Soc.* **1981**, *103*, 5039.
(54) Schaefer, J.; Stejskal, E. O.; McKay, R. A.; Dixon, W. T. *J. Magn. Reson.* **1984**, *57*, 85.
(55) Pochan, J. M.; Gibson, H. W.; Froix, M. F.; Hinman, D. F. *Macromolecules* **1978**, *11*, 165.
(56) Bondi, A. *J. Phys. Chem.* **1964**, *68*, 441.
(57) Bloom, M.; Davis, J. H.; Valic, M. I. *Can. J. Phys.* **1980**, *58*, 1510.
(58) Barbara, T. M.; Greenfield, M. S.; Vold, R. L.; Vold, R. R. *J. Magn. Reson.* **1986**, *69*, 311.
(59) Torchia, D. A.; Szabo, A. *J. Magn. Reson.* **1982**, *49*, 107.
(60) Spiess, H. W.; Sillescu, H. *J. Magn. Reson.* **1981**, *42*, 381.
(61) Tekely, P.; Turska, E. *Polymer* **1983**, *24*, 667.
(62) Sundararajan, P. R. *Can. J. Chem.* **1985**, *63*, 103.
(63) Tonelli, A. E. *Macromolecules* **1972**, *5*, 558.
(64) Erman, B.; Marvin, D. C.; Irvine, P. A.; Flory, P. J. *Macromolecules* **1982**, *15*, 664.
(65) Bendler, J. T. *Ann. N.Y. Acad. Sci.* **1981**, *371*, 299.
(66) Zorkii, P. M.; Razumaeva, A. E. *Zh. Strukt. Khim.* **1977**, *20*, 390.
(67) Gavezzotti A.; Simonetta, M. *Chem. Rev.* **1982**, *82*, 1.
(68) *Encyclopedia of Polymer Science and Engineering*; Wiley-Interscience: New York, 1988; Vol. 11, p 681.
(69) Roy, A. K.; Inglefield, P. T.; Shibata, J. H.; Jones, A. A. *Macromolecules* **1987**, *20*, 1437.
(70) Petrie, S. E. B.; Moore, R. S.; Flick, J. R. *J. Appl. Phys.* **1972**, *43*, 4318.
(71) Robeson, L. M. *Polym. Eng. Sci.* **1969**, *9*, 277.
(72) Robeson, L. M.; Foucher, J. A. *J. Polym. Sci., Polym. Lett. Ed.* **1969**, *7*, 35.
(73) Wyzgoski, M. G.; Yeh, G. S.-Y. *Polym. J. (Tokyo)* **1973**, *4*, 29.
(74) Dunitz, J. D.; White, D. N. *Acta Crystallogr.* **1973**, *A29*, 93.
(75) Schaefer, J., personal communication.

Cooperative Diffusion of Semidilute Polyelectrolyte Solutions: Analysis by Renormalization Group Theory

Lixiao Wang and Victor A. Bloomfield*

Department of Biochemistry, University of Minnesota, St. Paul, Minnesota 55108.
Received October 26, 1988; Revised Manuscript Received December 9, 1988

ABSTRACT: The renormalization group theory of Oono et al. for the concentration dependence of the cooperative diffusion of neutral polymer in semidilute solutions is applied to the polyelectrolyte sodium poly(styrenesulfonate) (NaPSS) in aqueous salt solution. This theory predicts that the reduced diffusion coefficient $D_c(C)/D_c(0)$ is a universal function of the reduced concentration A_2C, where A_2 is the thermodynamic second virial coefficient. It satisfactorily explains the experimental results of Koene et al. and Wang et al. over a range of salt concentrations from 0.01 to 0.15 M in semidilute solution. The low salt behavior of NaPSS is that expected in a good solvent, while that observed at higher salts shows a trend toward Θ solvent behavior. In dilute NaPSS solutions with low salt, the diffusion coefficient is overestimated compared to renormalization group theory predictions, perhaps due to chain expansion beyond the neutral good solvent limit. A plot of $D_c(C)/D_c(0)$ versus KC, where K is the diffusion virial coefficient, gives universal behavior characteristic of the good solvent limit over the entire concentration range, independent of polymer molecular weight or salt concentration. However, experimental uncertainties in K limit the reliability that may be ascribed to this result.

Introduction

This short report applies the renormalization group theory by Oono et al.[1,2] to the concentration dependence of the cooperative diffusion of semidilute polyelectrolyte solutions over a 15-fold range of salt concentrations. It shows that cooperative diffusion in semidilute polyelectrolyte solutions can be explained not only by scaling theory but also by the renormalization group theory.

The renormalization group theoretical approach has been successful in describing static properties of dilute[3,4] and semidilute[5,6] neutral polymer solutions. Transport properties of dilute solutions have also been studied[7] with the aid of the renormalization group theory. Wiltzius et al.[8] studied static and dynamic properties of polystyrenes in good and marginal solvents and found that the product of molecular weight (M) and osmotic compressibility (the derivative of the osmotic pressure (π) with respect to concentration (C), $M(\partial\pi/\partial C)T$, is a universal function of scaled concentration, independent of solvent quality and molecular weight. They also found that the ratio of dynamic length (ξ_H) to hydrodynamic radius (R_H) is a function only of the reduced concentration, KC, where K is determined from a virial expansion of the diffusion coefficient. Very recently, the cooperative diffusion constant in good solvents has been studied with the aid of the renormalization group methods based on the conventional minimal model—that model which takes into account the chain connectivity, the excluded volume interaction, and the hydrodynamic interaction (or the fluctuation of the solvent velocity field) by Oono et al.[1,2] The results agree well with the experimental results of Wiltzius et al.[8] Burchard[25] has described the static and dynamic properties of linear and star polystyrene and other polymers in terms of the renormalization group theory.

The situation with regard to polyelectrolytes is much less well developed, owing to complications arising from long-ranged polyion–polyion and polyion–small ion electrostatic interactions. Despite these difficulties, interest in polyelectrolyte dynamics has been considerable,[9,10] and certain aspects of the scaling theories of polyelectrolyte solutions have been established.[11-14] Several dynamic light scattering studies of polyelectrolytes have already been reported in the literature.[9,10,16-22] Many have reported the observation of a fast cooperative diffusion coefficient, D_c(fast), and a slow diffusion coefficient, D_c(slow), under low salt conditions.[9,10] Koene et al.[16] and Grüner et al.[19] reported on the polyelectrolyte concentration dependence of cooperative diffusion coefficients, which agrees reasonably well with the theoretical predictions of scaling theory. Wang et al. studied polyelectrolyte and salt concentration

0024-9297/89/2222-2742$01.50/0